Ge/Si Quantum Dot Formation from Non-Uniform Cluster Fluxes

Amanda E. Rider, Igor Levchenko, Kostya Ostrikov,* Michael Keidar

The controlled growth of ultra-small Ge/Si quantum dot (QD) nuclei (≈1 nm) suitable for the synthesis of uniform nanopatterns with high surface coverage, is simulated using atom-only and size non-uniform cluster fluxes. It is found that seed nuclei of more uniform sizes are formed when clusters of non-uniform size are deposited. This counter-intuitive result is explained via adatom-nanocluster interactions on Si(100) surfaces. Our results are supported by experimental data on the geometric characteristics of QD patterns synthesized by nanocluster deposition. This is followed by a description of the role of plasmas as non-uniform cluster sources and the impact on surface dynamics. The technique challenges conventional growth modes and is promising for deterministic synthesis of nanodot arrays.

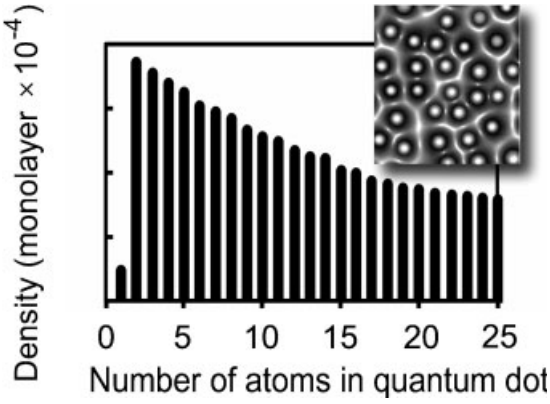

Introduction

Semiconducting quantum dots (QDs) have a variety of applications in a number of different fields including biomedical engineering, micro- and optoelectronics, quantum computing, data storage, quantum dot cellular automata, nanoplasmonics and semiconductor lasers.[1,2] There is a continuing demand for efficient and precise, yet simple QD deposition methods that are capable of meeting the essential requirements for nanodevice-grade QD patterns,[3,4] which include nanodot ordering and size uniformity within the pattern, as well as controlled size, crystallinity, and high surface coverage. Controlled delivery of building units from the nanofabrication environment and their self-assembly into surface nanopatterns is a commonly accepted and promising pathway to achieve this as yet elusive goal – specifically, achieving a high and uniform surface density (approaching one monolayer) consisting of ultra-small (<10 nm), size-uniform quantum dots. It presently appears quite challenging, if indeed possible at all, to direct QD self-assembly, which strongly depends on the surface energy and the lattice mismatch. Quantum dot nanopatterns usually develop via an island nucleation [Volmer-Weber (VW)], or a strain-driven fragmentation of a few-monolayer continuous film [Stranski-Krastanov (SK)] mechanisms.[5] Figure 1 shows the ranges of non-dimensional surface energy and lattice mismatch in epitaxial systems where such growth modes prevail. However, in both modes, the controllability of the QD areal density and uniformity is very limited. In fact, adatom nucleation in a VW mode produces nanopatterns with a broad variation in QD sizes, whereas fragmentation of continuous films into nanoislands in the SK mode is even less predictable, owing to its strong dependence on the number of monolayers and other factors. Moreover, it is still unclear how to grow QDs in lattice-matching systems with a high surface energy, which favor the layer-by-layer Frank-van der Merwe (FM) growth scenario (Figure 1).

A. E. Rider, I. Levchenko, K. Ostrikov
Plasma Nanoscience@Complex Systems, School of Physics, The University of Sydney, NSW 2006, Australia
Fax: +61 2 9351 7726; E-mail: K.Ostrikov@physics.usyd.edu.au
M. Keidar
Department of Aerospace Engineering, University of Michigan, Ann Arbor, MI 48109, USA

Plasma Process. Polym. **2007**, *4*, 638–647

DOI: 10.1002/ppap.200700043

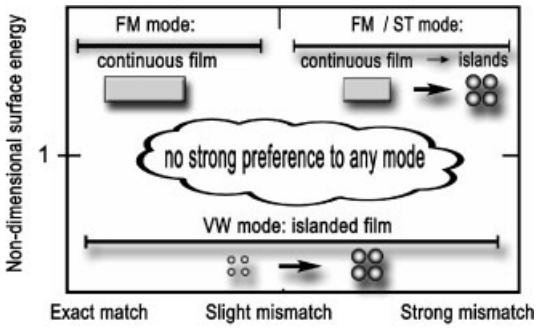

Figure 1. Ranges of favoured growth mode in terms of non-dimensional surface energy and lattice mismatch. In this paper the medium zone (no strong preference to any mode) is simulated.

Above all, it is still not certain what should be done under conditions that do not have a strong preference for any specific growth mode (area in the middle in Figure 1).

One possible way to solve this problem is to create a pattern of QD nuclei (QDN) suitable for subsequent growth of the desired QD array. Existing techniques based on intentional surface defects,[6] would fall short due the need to decrease the density of surface defects down to a value of $\approx 10^{10}$ m^{-2} or lower.[7] Other techniques such as nanoporous patterns,[8] or atom-by-atom manipulation would fail due to insufficient resolution.[9] Another possibility is to deliver beams of size-uniform seed nuclei, as it is commonly used in cluster beam deposition techniques.[10] However, even in this case, the seed sizes often appear quite non-uniform despite a uniform cluster delivery. This provokes an obvious question: do the gas-borne nanoclusters have to be of uniform size? Here, by means of numerical simulations, we present a counter-intuitive strategy for creating size-uniform QD nanopatterns by using fluxes of size-non-uniform clusters. The size-non-uniform building units then act as seed nuclei for the construction of the desired QD nanopatterns via controlled self-assembly. Whilst such cluster distributions may be generated from a range of sources,[11] utilising nanocluster-generating plasmas affords a number of advantages, from increased control of the clusters production, to transportation via the plasma sheath to the deposition surface, not to mention the surface energetic considerations such as the impact on diffusion rates.[12] The viability of plasma processing in the fabrication of nanostructures, protective coatings and a range of biomedical applications is therefore evident.[13–18] Low temperature non equilibrium plasma processing in particular, is attractive for the fabrication of a wide range of materials,[17] notably low dimensional nanostructures such as binary SiC quantum dots.[19] Another prominent example is the plasma enhanced chemical vapour deposition (PECVD) of polymer coatings.[20] As mentioned, plasmas possess many favourable properties that can be used to aid and advance nanofabrication efforts; for example, the wide range of species in a typical plasma discharge may be exploited as building units (BUs) in carbon nanotube production.[18]

Our model and numerical details are presented in Section 2. Section 3 consists of an analysis of our results and their relation to available experimental results, followed by an indepth discussion of the role of plasmas as a non-uniform cluster source, the impact they have on surface diffusion processes and hence the advantages inherent in adopting a plasma-based process over a neutral gas-based route for the production of size uniform QD patterns.

Model and Computational Method

Model Formulation

We consider Ge/Si QDs, one of the most popular QD systems[21,22] with a moderate (≈4%) lattice mismatch. This system is commonly grown using a variety of neutral gas processes such as chemical vapour deposition and molecular beam epitaxy, and it typically develops via the SK mechanism, which comes into play after a few monolayers have been epitaxially grown.[23] Here we propose an alternative method wherein size non-uniform nanoclusters are delivered alongside atomic/ionic BUs, which self-assemble and create the desired QDN[1] pattern on a Si(100) surface. To show this, we simulate and compare the initial stage of Ge/Si QD pattern formation on the Si surface exposed to an atom/ion only flux and two different atom/ion/nanocluster fluxes (Figure 2a), henceforth referred to as the atom-only route and non-uniform cluster routes (NUC and NUC2), respectively. The nanocluster fluxes considered include clusters of up to 25 atoms. For the atom-only route, we used a flux absent of any nanoclusters, whereas for the NUC and NUC2 cases, size non-uniform nanocluster fluxes as shown in Figure 2b were used which are typical for the low-temperature plasmas.[24,25] It should be noted that the species included in our model for the NUC and NUC2 fluxes were restricted to atoms, monatomic Ge ions and neutral clusters consisting of one to twenty atoms. We quantify how using a size-non-uniform cluster influx affects the QDN and we show the advantages in formation of size-uniform patterns of QDN offered by the non-uniform cluster route. The QDN pattern formation was simulated separately for the atom-only, NUC and NUC2 fluxes.

[1] Note we use the term QDN to refer to a cluster of atoms on the substrate, this is to avoid any confusion between clusters forming on the surface and the nanoclusters delivered via the NUC and NUC2 influxes.

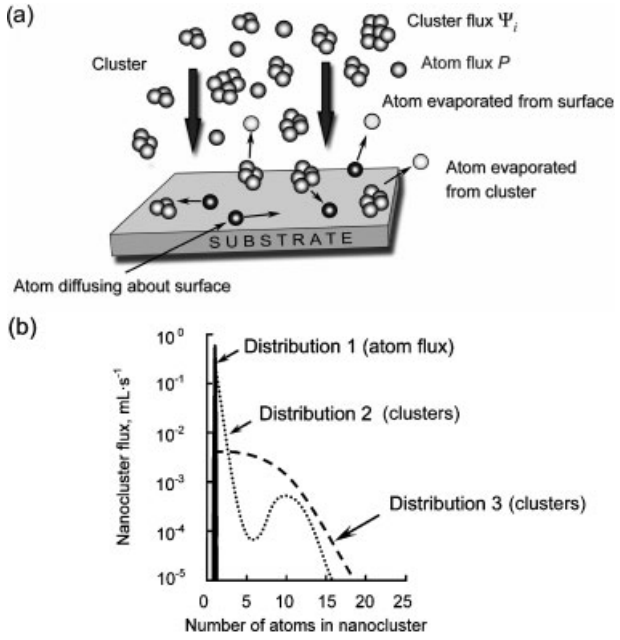

Figure 2. a) Main processes on substrate surface during quantum dot deposition from atom and nanocluster-containing fluxes; b) atom-only flux (Distribution 1), nanocluster-containing flux for NUC2 process (Distribution 2) and nanocluster-containing flux for NUC process (Distribution 3) used in simulations.

We have assumed a stress- and defect-free surface. This is well justified for the moderate lattice mismatch and very low ($\approx 10^{-4}$ ML) surface densities considered. The QDN densities examined here (e.g. a rough estimate for a QD of approx 10 nm with a spacing of 20 nm between QDN centres, on a substrate with lattice density 4×10^{18} m^{-2}, implies a QD density of 2.5×10^{15} m^{-2}) are significantly higher than the highest surface defect densities acceptable in microelectronics,[6] which, as we have stated previously, is $\approx 10^{10}$ m^{-2}. Given that the number of islands formed equals the number of defects, this implies that QD fabrication techniques based on intentional surface defects will not be capable of producing the dense QD patterns that we are interested in. Our model takes the main processes of BU delivery and consumption on the surface into account.[19,26] Building units are delivered to the seed formation sites by diffusion about the surface and are consumed by adatom attachment to the growing seeds. The surface density η_i (m^{-2}) of QDN consisting of (i) atoms (where $i > 1$) can be obtained from:

$$\frac{\partial \eta_i}{\partial t} = \Psi_i + \dot{\eta}_{i.C} + \dot{\eta}_{i.2D} + \dot{\eta}_{i.3D}, \quad (1)$$

where $\frac{\partial \eta_i}{\partial t}$ is the change in density [m$^{-2} \cdot$ s^{-1}] of (i)-atom QDN and Ψ_i is the deposition rate of clusters [m$^{-2} \cdot$ s^{-1}] consisting of (i) atoms ($i > 1$),

$$\dot{\eta}_{i.C} = 2\upsilon_d \eta (r_{i-1}\eta_{i-1} - r_i \eta_i), \quad (2)$$

is the rate of density variation of nanoclusters [m$^{-2} \cdot$ s^{-1}] consisting of (i) atoms due to adatom collisions with nanoclusters consisting of (i) and (i-1) atoms,

$$\dot{\eta}_{i.2D} = \eta_{i+1} n_{i+1} \nu_{i+1} - \eta_i n_i \nu_i, \quad (3)$$

is the rate of nanocluster density variation due to atom evaporation to the 2D (surface) vapour from nanoclusters consisting of (i) and ($i+1$) atoms, and

$$\dot{\eta}_{i.3D} = \pi \eta_k (r_{i+1}^2 \eta_{i+1} \mu_{i+1} - r_i^2 \eta_i \mu_i), \quad (4)$$

is the rate of nanocluster density variation due to the atom evaporation to the 3D (external) vapour from nanoclusters consisting of (i) and ($i+1$) atoms. Other variables used in Equation (2)–(4) are as follows: η is the surface density of adatoms [m$^{-2} \cdot$ s^{-1}], $\upsilon_d = \lambda_S \ \nu_0 \ exp(-\varepsilon_d/kT)$ is the adatom surface diffusion rate [m $\cdot$ s^{-1}], λ_S is the lattice parameter [m] for the silicon substrate, $\nu_0 = 2kT/h$ is the lattice atom oscillation frequency [s^{-1}], k is Boltzmann's constant, h is Planck's constant, T is the surface temperature [K], ε_d is the surface diffusion activation energy [eV], r_i is the radius [m] of QDN consisting of (i) atoms, n_i is the number of atoms at the border of QDN consisting of (i) atoms, $\eta_k = 1/\lambda S2$ is the surface density of Si atoms on the substrate surface, $\nu_i = \nu_0 \ exp(-\varepsilon_{b \cdot i}/kT)$ is the rate of atom evaporation [s^{-1}] to the 2D (surface) vapour from borders of QDN consisting of (i) atoms, $\varepsilon_{b \cdot i}$ is the energy of atom evaporation to the 2D (surface) vapour from borders of QDN consisting of (i) atoms, $\mu_i = \nu_0 \ exp(-\varepsilon_{a \cdot i}/kT)$ is the rate of atom evaporation to the 3D vapour from surface of QDN consisting of (i) atoms, and $\varepsilon_{a \cdot i}$ is the energy of atom evaporation to the 3D vapour from surface of QDN consisting of (i) atoms.

The balance of adatom density on the solid surface is described by

$$\frac{\partial \eta}{\partial t} = P + P_{ne} - P_e - P_{na}, \quad (5)$$

where P is the external flux of atoms [m$^{-2} \cdot$ s^{-1}] to the substrate surface,

$$P_{ne} = \sum_2^\infty n_i \eta_i \nu_i, \quad (6)$$

is the flux of atoms evaporating from the QDN borders to the 2D vapour on the substrate surface,

$$P_e = \eta \cdot \nu_0 \cdot \exp(-\varepsilon_a/kT), \quad (7)$$

DOI: 10.1002/ppap.200700043

is the flux of adatoms evaporating from the substrate surface, ε_a is the energy of Ge adatom evaporation from the substrate (Si) surface, and

$$P_{na} = 2\eta\upsilon_d \sum_{i=2}^{\infty} r_i\eta_i, \quad (8)$$

is the flux of adatoms attaching to QDN.

The evaporation energies $\varepsilon_{a\cdot i}$, $\varepsilon_{b\cdot i}$, and QDN radius r_i depend on the QDN size. We have assumed here that the quantum dots are hemispherical (this is close to the shapes observed in experiments[27]), and thus the energies were calculated by taking into account the number of bonds between the atoms constituting the QDN. Thus, for Ge atom evaporation to the 2D vapour we obtain: for $i=2$, $\varepsilon_{b\cdot 2}=\varepsilon_b$ (1 bond); for $i=3$, $\varepsilon_{b\cdot 3}=2\varepsilon_b$ (2 bonds); for $i=4$, $\varepsilon_{b\cdot 4}=2\varepsilon_b$ (2 bonds) etc. approaching $\varepsilon_{b\cdot i}=½\boldsymbol{\varepsilon_{a\cdot Ge}}$ for $i=>\infty$, where $\boldsymbol{\varepsilon_{a\cdot Ge}}$ is the energy of atom evaporation from the surface of bulk Ge. For evaporation from a 2-atom nucleus to the 3D vapour, a Ge atom should spend the energy ε_b for breaking one bond with a Ge atom in addition to the energy ε_a for breaking the bond with the surface; we recall here that the model considers quantum dot nuclei that consist of a discrete number of atoms and thus exhibit properties that depend discretely on the size. Therefore, the energy of Ge atom evaporation to the 3D vapour from the surface of QDN consisting of (i) atoms is: $\varepsilon_{a\cdot 2}=\varepsilon_b+\varepsilon_a$ for $i=2$; similarly, $\varepsilon_{b\cdot 3}=2\varepsilon_b+\varepsilon_a$ for $i=3$; $\varepsilon_{a\cdot 4}=3\varepsilon_b-\varepsilon_a$ for $i=4$; etc., approaching $\varepsilon_{a\cdot i}=\varepsilon_{a\cdot Ge}$ for $i=>\infty$, where $\varepsilon_{a\cdot Ge}$ is the energy of Ge atom evaporation from the surface. The number of atoms at the QDN border n_i was also determined by analyzing the QDN geometrical shape: $n_2=2$, $n_3=3$, $n_4=4$, $n_5=4$, etc., approaching $n_i=4.83i^{1/3}$ for $i=>\infty$.

In simulations, we used the surface diffusion activation energy ε_d, evaporation energy ε_a, and bonding energy ε_b, as well as the lattice parameter λ_S representative of the Ge/Si(100) system:[28–32] $\varepsilon_d=0.67$ eV, $\varepsilon_a=2.69$ eV, $\varepsilon_b=1.5$ eV, $\boldsymbol{\varepsilon_{a\cdot Ge}}=3.5$ eV, and $\lambda_S=5.4\times10^{-10}$ m. The substrate temperature was $T=600$ K, the total QDN surface density $\rho=0–2\times10^{-3}$ monolayers (ML), total external flux of atoms $P=1–10$ ML/s, and the mass of nanoclusters $m=72–1\,800$ amu.

Numerical Details

We recall here that our aim is to simulate the very initial stage of the quantum dot array formation; thus we integrated the set of Equation (1)–(6) with zero initial conditions ($\eta=0$ and $\eta_I=0$ at $t=0$), i.e. we start the computations with a clean uncoated surface. The simulation domain (substrate surface) was assumed to be infinite. The simulation process was stopped when the number of atoms in the quantum dot nuclei reached 25–30. At this stage, the initial pattern is formed, the rate of new QDNs formation decreases significantly, and the kinetic approach used here for the description of adatom attachment to the quantum dots becomes inadequate. Quantum dots consisting of (i) atoms ($i>1$) were formed by adatom attachment to QDs consisting of (i–1) atoms, adatom evaporation to the 2D and 3D vapours from ($i+1$)-atom QDs. Recall the formula for diffusion rate, $\upsilon_d=\lambda_S\cdot\nu_0\ exp(-\varepsilon_d/kT)$, in particular note the diffusion activation energy in the exponent. For clusters, the diffusion activation energy is higher, for example, in the case of 2-atom clusters – the activation energy is doubled, this results in a prohibitively low surface diffusion rate which is further exacerbated for larger clusters. Therefore, we neglect cluster migration and assume that adatoms are the only species incident on the substrate with an appreciable mobility that may add to, evaporate or detach from QDN. Clusters consisting of two or more atoms are treated as immobile once they have landed on the substrate. Attachment of atoms/ions from the BU flux directly to the QD itself was neglected due to the small surface coverage considered. Indeed, with the total surface density of all quantum dot nuclei not exceeding 10^{-3} ML and number of atoms in quantum dots of about 25, the surface coverage by the quantum dot nuclei does not exceed 10^{-2}, thus providing a low error (1%) due to neglecting the direct atom attachment. During the simulation, a variable time step was used, which was chosen at each step to provide a small enough (not exceeding 1%) increment of the density of QDNs that would demonstrate a maximal rate of growth. All time-dependent material characteristics were recalculated after each time step. The quantum dot seed distribution function was calculated at the end of the initial stage of the simulation process. To explicitly show the advantage offered by the NUC route over the atom-only route in generating size-uniform patterns of nanosized quantum dots, we have conducted (after obtaining the distribution of the quantum dot nuclei) a further computation examining quantum dot growth using a standard diffusion model, with the sole aim being to demonstrate how the difference between the two QDN patterns formed from these fluxes (atom only and NUC) impacts on the further evolution of the quantum dot pattern. We did not study the detailed characteristics of the final quantum dot nuclei pattern here, and, instead, we have computed only the distributions of the more evolved quantum dots in fully developed patterns. The computations were made using a diffusion model within the ranges of QD surface coverage up to 0.25 and quantum dot radii 5–10 nm. The model is based on a standard diffusion equation of adatoms on the substrate surface.[33] Obtaining the density of adatoms on a surface from such an equation is straightforward, the

quantum dot growth may then be described using a standard growth equation.[33] This approach allows us to model the pattern development to larger (up to several tens of nm) quantum dots in the adatom-diffusion approximation. The details of this model are not considered here and can be found elsewhere.[34,35]

Results and Discussion

Physical Interpretation

Figure 3a–5a shows the temporal evolution of the surface densities of adatoms and QDN consisting of 2 to 10 atoms computed for the atom-only and NUC cases. For the atom-only process, as observed in Figure 3a, all densities increase for the first 10 μs, and then tend to saturate. During the first several μs, smaller QDN have higher densities, but between 15 and 25 μs, the ordering of densities gradually changes and becomes inverted: the QDN consisting of 10 atoms now have the highest densities, whereas the adatoms and 2-atom QDN have the lowest. The two most striking observations in the NUC case (Figure 4a) are the very strong fall of adatom density and the similar behaviour exhibited by the densities of all QDN during the first 10 μs. Between 0 and 25 μs, the difference between the densities of the QDN and adatoms reaches approximately 2 orders of magnitude. The temporal evolution of surface densities for the NUC2 case is presented in Figure 5a. The QDN densities rapidly increase during the first 5 μs, and then tend to saturate at levels dependant on the number of atoms involved in the QDN. At the early stage (≈5 μs), the density of adatoms exceeds that of i-atom QDN ($i > 1$). Thereafter, it decreases rapidly and becomes lower than any QDN density. It can be

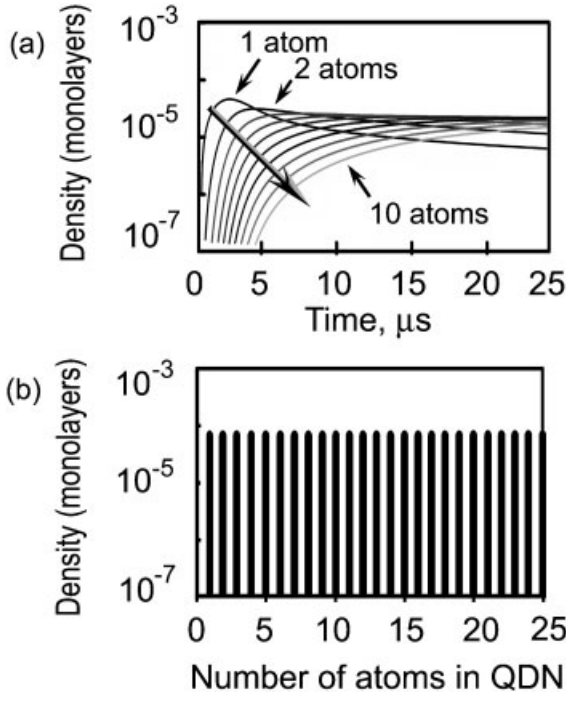

Figure 3. a) Temporal evolution of QDN surface density in the atom-only case; b) final QDN distribution function. Large arrow in a) shows the direction of the QDN mass increase.

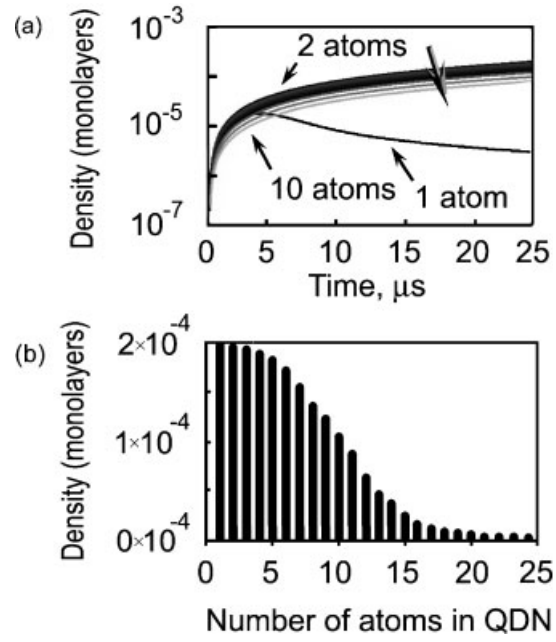

Figure 4. Same as Figure 3 for the NUC case.

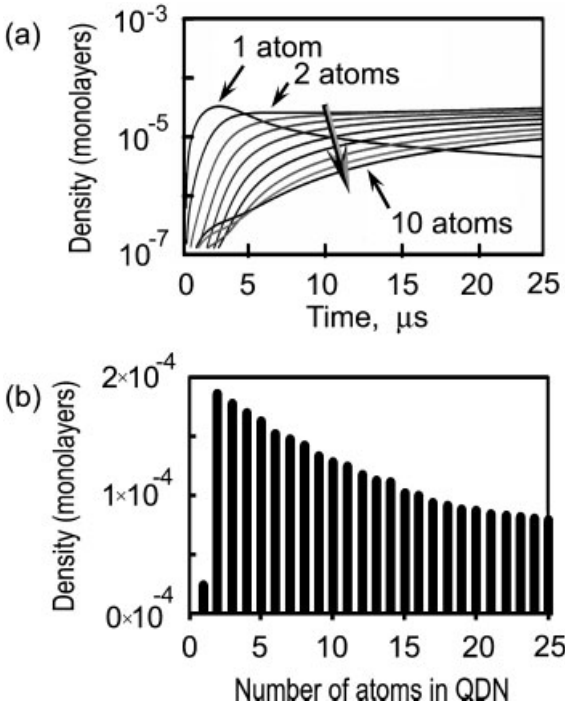

Figure 5. Same as Figure 3 for the NUC2 case.

DOI: 10.1002/ppap.200700043

observed through Figure 5a that, during the entire period of simulation, there was an inverse relationship between the QDN densities and the number of constituent atoms, i.e., densities of smaller QDN always remained higher. Corresponding equilibrium QDN distributions (taken at 1 ms) are presented in Figure 3b–5b. The QDN size distribution taken at equilibrium for the atom-only case is a uniform function, in which the numbers of the smallest and largest QDN are approximately equal (Figure 3b). Figure 4b reveals that the equilibrium distribution function of QDN deposited from the NUC flux exhibits a very strong decrease in the density of QDN consisting of 15–20 atoms. The density of QDN of 20 atoms is approximately 10 times lower than that of QDN consisting of 2 and 3 atoms, whereas the density of quantum dot nuclei consisting of 25 atoms and more approaches zero (Figure 4b). The NUC2 QDN distribution function (Figure 5b) yields a similar result, albeit with a significantly less pronounced decrease, it exhibits a clear descending shape; the decline is rather strong and covers approximately one order of magnitude. In fact, the density of QDNs consisting of 2 and 3 atoms is approximately double that of 25 atom-nuclei by ($\approx 2 \times 10^{-4}$ versus $\approx 1 \times 10^{-4}$ ML). The decrease is observed to be almost a linear function. The surface coverage in the atom-only process is lower than both the NUC and NUC2 cases.

Comparison of the distributions of the QDN obtained in the atom-only (Figure 6a and b) and NUC (Figure 6c and d)) processes evidences a major advantage of the NUC-based synthesis of a dense QDN pattern suitable for further growth of the uniform QD array with high surface coverage. Indeed, by using this process, one can deposit a high-density seed pattern of small (<15 atoms) QDN (Figure 6c and d). Further growth of these QDN results in the formation of a high-surface-coverage pattern of QDs of approximately the same size (Figure 6d), note that Figure 6b and d were both produced using the diffusion model described in the numerical details section. In contrast, the atom-only flux grown QDN patterns feature a large number of QDN consisting of 25 or more atoms. The accelerated growth of such large seed nuclei results in a suppression of the growth of smaller QDN, which are eventually dissolved via 2D evaporation (a number of smaller QDN in the process of dissolution via 2D evaporation can be readily observed in Figure 6b). Thus, the density of QD patterns formed from an atom-only flux (Figure 6b) is in fact lower than that formed via the NUC process.

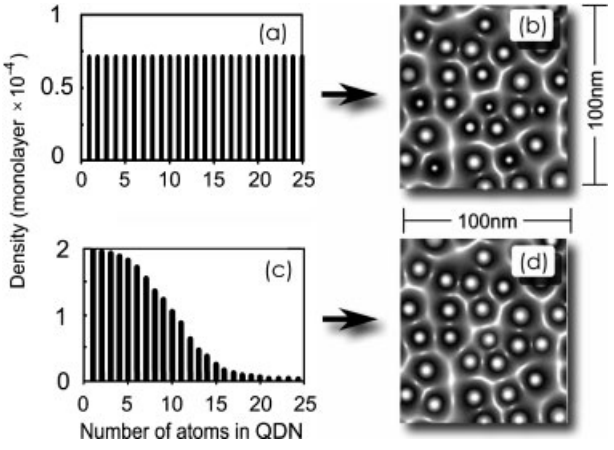

Figure 6. Size distributions and simulated patterns of quantum dot nuclei: a, b): deposition from atom only flux; c, d): Deposition from NUC flux. Substrate wafer dimensions ≈100 nm × 100 nm.

From the nanofabrication perspective, a dense nanopattern of same-size QDNs is an important prerequisite in obtaining dense arrays of nanodots of the same size; that is why our aim is to minimize the width of the QDN size distribution. The result obtained in the atom-only process is apparently the worst from this point of view. When using non-uniform clusters, on the other hand, one can expect a much more uniform QD growth, which will develop from seed nuclei of more-or-less similar size (<15 atoms). The abrupt cut-off in the number densities of large QDN reduces the chances of the growth of over-sized QDs, thus ensuring a substantial improvement of the quality of the entire nanopattern.

Remarkably, the QDN distributions on the surface do not mirror the BU distributions in the gas phase. Indeed, in the atom-only process, a narrow building unit distribution results in a broad spectrum of seed nuclei sizes. Conversely, broader BU size distributions in the NUC and NUC2 sources lead to much narrower QDN size distributions on the surface. We thus arrive to a counter-intuitive conclusion, namely, that the synthesis of size-uniform QDN nanopatterns may not necessarily require an influx of size-uniform BUs as is commonly believed.

What is also interesting is the difference between the NUC and NUC2 results. In the NUC2 case, the distribution contains relatively weaker fluxes of smaller nanoclusters (consisting of 3–10 atoms) and intense fluxes of atoms/ions and very small nanoclusters (consisting of 2 and 3 atoms). In the NUC process, mostly small clusters of 2–10 atoms are delivered. Surprisingly, despite the similar involvement of larger (>10 atoms) nanoclusters (Figure 2b), the quantum dot nuclei distribution functions on the surface (Figure 4b and 5b) are quite different. This difference can be attributed to different kinetic scenarios of adatom self-organization on the substrate surface. The NUC2 distribution (Curve 2 in Figure 2b) provides an increased influx of atoms and ions incident to the substrate that become adatoms upon landing and subsequently control the evolution of the QDNDF. In this case the adatom density is high and larger nanoclusters deposited directly to the substrate will grow via adatom

incorporation. Furthermore, adatoms re-evaporated from smaller QDNs to the 2-D vapor can also play a very important role in the pattern formation. Eventually, intense adatom-QDN interactions compensate for the 'pit' in the NUC2 influx distribution function, and yield a relatively uniform distribution of the QDNs on the surface. In the NUC process, however, the density of adatoms on the surface is much lower. This causes a notable reduction of the QDN growth rates. Likewise, re-evaporation and selective attachment of adatoms to different QDN strongly affect the nanopattern development. As a result, the originally uniform pattern of quantum dot nuclei is affected by the retarded growth of larger QDN and evolves into a pattern with substantially reduced densities of large seed nuclei. In most existing neutral gas-based techniques Ge/Si(100) QDs follow the SK growth scenario,[36] which is very sensitive to the surface state, stresses, and other conditions. This is why it is nearly impossible to control the fragmentation of a continuous film, which leads to ripening of Ge/Si quantum dots – that is, consumption of smaller QDs in favour of large QD formation. Clearly, as seen through Figure 4b and 5b, the final QD pattern is sensitive, not only to the presence of non-uniform clusters but also to their specific size distribution in the influx. Here, we have introduced an alternative pathway, where the density and sizes of the QD seed nuclei can be controlled by the building unit composition and size distribution in the NUC flux. A specific recipe is to use a reduced atom influx to the substrate, thus reducing the adatom density and hence avoiding uncontrollable formation of the QDN pattern from diffusing adatoms, and to have a controllable influx of size-non-uniform nanoclusters. In this way, one can create an initial pattern for the deposition of a quantum dot array with the required surface coverage. Note that in coventional SK growth, an atom flux is deposited on the substrate, leading to the formation of a few monolayers. The strain induced fragmentation of these monolayers (a result of the lattice mismatch of the system) is what causes the formation of large islands, with further growth via by adatom diffusion. The method examined in this paper differs in that clusters, as well as atoms/ions are delivered to the deposition surface; the presence of these clusters act as 'already separated film fragments' effectively frustrating the strain-induced fragmentation favoured by SK growth. To estimate the final surface coverage by the quantum dots grown from the computed QDN pattern, we assumed the final QD radius of $R_n = 6$ nm, and determined (by integrating the distribution function) the total density of all QDN (i.e. QDNs of all sizes) that is equal to $\approx 10^{-3}$. Thus, the step between QDN on surface is 15 nm, and the surface coverage for the final QD pattern reaches 0.5. Hence, if the quantum dots continue to develop smoothly (without coalescence), the required nanopattern density and QD size distribution can be achieved deterministically.

Analysis of Relevant Experimental Data

Strong support for the model and numerical simulations can be obtained by analyzing available experimental data on the dependence of islanded film morphology on the distribution of nanoclusters in the incoming flux. The experiments convincingly support our most important finding, namely the counter-intuitive fact that the use of a NUC flux incorporating larger nanoclusters leads to formation of denser patterns of the quantum dots of smaller size. The deposition of antimony films of a thickness of 1 and 5 nm,[37] as well as 10 nm[38] has revealed a striking advantage of nanocluster deposition over atom flux deposition in terms of uniformity of the fabricated nanopatterns. More importantly, our numerical results appear to be in a fair agreement with the experimental findings. This is evidenced by the comparison of the parameters of the quantum dot nanopatterns derived from numerical simulations in this work with the relevant experimental data[37] (Table 1).

Table 1. Comparison of calculated and experimental values of difference in nanoislands size and in surface coverage for atom and nanocluster flux, equivalent film thickness 5 nm.

Parameter		Value	Ref.
Difference in nanodot size, $d_{max} - d_{min}$, nm	Atom/molecular flux	70	From Figure 2e, ref. [37]
		56	Calculated (this work)
	Nanocluster flux	5	From Figure 2f, ref. [37]
		4	Calculated (this work)
Surface coverage	Atom/molecular flux	0.15	From Figure 2e, ref. [37]
		0.2	Calculated (this work)
	Nanocluster flux	0.5	From Figure 2f, ref. [37]
		0.47	Calculated (this work)

Plasma Process. Polym. **2007**, *4*, 638–647

DOI: 10.1002/ppap.200700043

However, experimental verification of the very initial stage of QDN pattern development is extremely challenging. It is worth emphasizing that despite impressive recent advances in nanofabrication and analytical surface science/materials science techniques, at this stage an experimental investigation of the very short transition processes (up to ≈25 μs) of our interest here seems to be quite difficult, if indeed possible at all. The main reason is the ultra-small (subnanometer) nanocluster sizes studied and their very short time scales of formation on the surface. Presently available atomic-resolution analytical tools of surface science and materials science[6] still cannot meet the strict requirements (e.g., adequate time resolution to scan sufficiently large surface areas with atomic (≈0.2 nm) precision and vacuum compatibility with plasma-based and other UHV processes) for time-resolved in situ measurements of the nanocluster size distributions computed in this work. Therefore, numerical experiments still remain the only viable way to investigate the initial (core structure-determining) stage of self-assembly of Ge/Si quantum dots on silicon surfaces.

The Role of Plasmas

The possible sources of size non-uniform clusters should be discussed. There are a number of environments conducive for preparing clusters – from neutral gases to complex, reactive plasmas. It is immediately clear from our results that precise control of cluster size distribution is essential in the fabrication of nanodevice-grade QDs. In the case presented in this paper, the most important element is therefore the ability to precisely tailor the cluster size distribution and the most promising pathway from this point of view is the plasma route.

The complex chemistry occuring in a typical plasma discharge results in the formation of a wide range of species that can act as potential building units: from atoms/ions/radicals/molecules to nanoclusters. The amount of each species produced, however, is largely dependant on how plasma parameters, such as working pressure, temperature, degree of ionisation, power, and composition of the precursor gas feedstocks can be manipulated to favour certain reactions taking place. Plasmas hold much promise in that specifically tailoring cluster distributions for a wide variety of deposition scenarios is not their sole function, they may also be used in surface preparation (energetic ions such as Ar^+, frequently included in plasma mixtures are commonly used to activate a deposition surface, similarly atomic hydrogen, also a common constituent is employed to terminate surface dangling bonds) in addition to controlling the transport of particles and clusters via the plasma sheath to the substrate.[3] The importance of plasmas in the generation and transport of BUs is clear, however, we are also interested in the influence plasmas exert on surface reactions. What must be considered in plasmas particularly, as opposed to neutral gas cluster sources, is the role of ions. Whilst not explicitly accounted for in this study (ions are assumed to become adatoms when they land on our substrate), ions significantly influence surface dynamics due to their effect on surface activation energy. The ionic charge used may be chosen such that the surface activation energy is lowered – making diffusion and associated surface processes increasingly energetically favourable and therefore more likely to occur.[12] Thus energetic ions can substantially increase surface reaction rates.[51] Given that surface diffusion is the dominant formation mechanism at the initial growth stage, this is very important indeed. In addition, it has been noted by Wegner et al.[11] that a requirement for clusters in nanostructured films is that they possess sufficient impact energy to dislodge a surface lattice atom in order to anchor the incident cluster to the surface. Roca i Cabarrocas et al.[39] noted that the impact energy of positively charged ultra-small Si nanoparticles may be controlled by applying a dc potential drop between the plasma and substrate.

For any technological application, QDs must be able to be fabricated in a uniform, regular array;[40] therefore correct placement of QDs is also a concern. An article by Krinke et al.[41] reveals that the presence of ionized species (as typically found in a plasma distribution) results in less agglomeration on the substrate, instead a more randomized distribution is obtained – this means less clumping in particular areas on the substrate. In the fabrication of other nanostructures, carbon nano-tips for example, the use of plasmas via PECVD has resulted in significantly better size and positional uniformity[42–44] than that recorded for the neutral gas – thermal CVD route. Similarly, it has been noted that the growth process of carbon nanotubes is dependant on the residence time of the plasma generated nanotube seed particles in the preferential growth region.[45,46] The use of ion fluxes has been noted as a way to reduce hydrogenation – leading to higher purity films and nanostructures.[47] Several authors[47–50] examined the effect of substrate heating by a plasma during PECVD, it was found that additional external heating was not required and actually proved detrimental. It was noted that in general, due to the greater dissociation of the feedstock gas by plasmas and thus to the greater variety of species for carbon nanotube growth, the growth temperatures for PECVD were ultimately lower than those required for thermal CVD (which employs a neutral gas route). Substrate temperature impacts on surface reactions, carbon dissolution and diffusion into metal particles, as well as playing a role in surface preparation. The lower growth temperatures employed when using non-thermal equilibrium plasmas open up the range of substrates that may be processed, including temperature sensitive materials such as polymer substrates.[20,51] Clearly, lowered

surface diffusion activation energies and higher substrate temperatures result in a higher diffusion rate (recall $\upsilon_d = \lambda_S \nu_0 \ exp(-\varepsilon_d/kT)$). The use of plasmas, therefore, is not restricted to the ability to precisely tailor the cluster size distribution; they are also particularly important in increasing the rate of surface diffusion, and by extension, the speed of the nanoassembly process.

The NUC distribution used in this article is very similar to the nanocluster size distribution representative of reactive silane plasmas,[25] such plasmas similarly include predominantly neutral clusters.[52] The NUC2 distribution is likewise similar to a numerical cluster distribution in low pressure silane plasmas.[24] Other plasma cluster sources, besides reactive plasmas (i.e. silane), include magnetron sputtering,[53] laser vaporization cluster source (LVCS), pulsed microplasma cluster source (PMCS) and pulsed arc cluster ion source (PACIS), amongst others.[11] The wide range of choices reinforces the observation that plasmas are effective tools for the whole spectrum of nanofabrication process. We reiterate that an indepth discussion of species production mechanisms via the myriad chemical reactions occurring in complex plasma discharges, and their subsequent modification via manipulation of plasma parameters represents a significant research effort by itself and as such is beyond the scope of this article. This article is intended as an exposition of the advantages inherent in using a non uniform cluster flux instead of an atom-only flux in the initial stage of QDN, not an extensive technical description of quantum dot fabrication at all stages from species generation, to surface preparation to the final QD product. Our simulation efforts, in addition to the above discussion, have conclusively demonstrated that partially ionized low-temperature non-equilibrium plasmas that can generate suitable non-uniform cluster distributions can be used to effectively control the nuclei nanopattern development, ultimately giving rise to size-uniform and dense seed patterns. Plasmas offer many competitive advantages for nanofabrication, most notably they may be used in every step of the nanofabrication process.

Conclusion

In summary, we have reported on a numerical simulation of Ge/Si quantum dot seed pattern formation from atom-only and non-uniform cluster fluxes. Our results demonstrate that the NUC flux provides a very narrow size distribution function of the quantum dots seed pattern, with a sharp decrease of the number of QDN consisting of 15 (or more) atoms. In the atom-only process, the seed size distribution is much wider and the numbers of QDNs consisting of 2–3 atoms is almost the same as the numbers of nuclei consisting of 25 atoms. Moreover, our numerical experiments suggest that the adatom density on the Si(100) surface in the NUC process can be very low; this suppresses the unwanted formation of new quantum dots during the growth process. The calculated parameters of nanodot patterns have been compared with relevant experimental data, and a reliable agreement was demonstrated. Having demonstrated the possibility of forming a very dense pattern (2×10^{-4} ML for smallest QDNs) with the final QDs coverage of 0.5 from NUCs, compared to density of 2×10^{-5} ML and final coverage of 0.2 for the atom-only case, we have proposed an alternative QD nanopattern formation method, which does not involve the commonly accepted Stranski-Krastanov route and in addition provides much greater process controllability. The immense potential of plasma processing as a promising and competitive fabrication environment for quantum dot arrays has been elucidated via our numerical experiment and extended discussion, serving both as a source for non-uniform clusters as well as influencing surface diffusion rates. Future directions[54–59] include refinement of this model for later growth stages, and increased focus on the role of surface charge due to plasmas, not only in the initial formation of these dots but also in the effect of ions on the deterministic placement of QDs in the uniform arrays required for technological applications.

Acknowledgements: This work was partially supported by the *Australian Research Council and the University of Sydney. A. E. R.* was supported by the *Australian Postgraduate Award* (APA).

Received: March 16, 2007; Revised: April 21, 2007; Accepted: April 30, 2007; DOI: 10.1002/ppap.200700043

Keywords: diffusion; nanostructures; nucleation; plasma nanofabrication; quantum dots

[1] X. Michalet, F. Pinaud, L. A. Bentolila, J. Tsay, S. Doose, J. Li, G. Sundaresan, A. M. Wu, S. S. Gambhir, S. Weiss, *Science* **2005**, *307*, 538.
[2] J. L. Gray, R. Hull, C. -H. Lam, P. Sutter, J. Means, J. A. Floro, *Phys. Rev. B* **2005**, *72*, 155323.
[3] K. Ostrikov, *Rev. Mod. Phys.* **2005**, *77*, 489.
[4] Y. Yin, A. P. Alivisatos, *Nature* **2005**, *437*, 664.
[5] G. S. Solomon, J. A. Trezza, A. F. Marshall, J. S. Harris, Jr., *Phys. Rev. Lett.* **1996**, *76*, 952.
[6] P. Jensen, *Rev. Mod. Phys.* **1999**, *71*, 1695.
[7] USA 5156995 (1992), invs.: E. A. Fitzgerald Jr., D. G. Ast.
[8] P. Chen, S. J. Chua, Y. D. Wang, M. D. Sander, C. G. Fonstad, *Appl. Phys. Lett.* **2005**, *87*, 143111.
[9] J. Liang, H. Chik, A. Yin, J. Xua, *J. Appl. Phys.* **2002**, *91*, 2544.
[10] L. Ravagnan, F. Siviero, C. Lenardi, P. Piseri, E. Barborini, P. Milani, C. S. Casari, A. Li Bassi, C. E. Bottani, *Phys. Rev. Lett.* **2002**, *89*, 285506.

DOI: 10.1002/ppap.200700043

[11] K. Wegner, P. Piseri, H. Vahedi Tafreshi, P. Milani, *J. Phys. D: Appl. Phys.* **2006**, *39*, R439.
[12] A. Anders, *J. Phys. D: Appl. Phys* **2007**, *40*, 2272.
[13] U. Cvelbar, M. Mozetic, M. K. Sunkara, S. Vaddiraju, *Adv. Mater.* **2005**, *17*, 2138.
[14] E. Sardella, R. Gristina, G. S. Senesi, R. d'Agostino, P. Favia, *Plasma Process. Polym.* **2004**, *1*, 63.
[15] E. Sardella, P. Favia, R. Gristina, M. Nardulli, R. d'Agostino, *Plasma Process. Polym.* **2006**, *3*, 456.
[16] S. Xu, J. Long, L. Sim, C.-H. Diong, K. Ostrikov, *Plasma Process. Polym.* **2005**, *2*, 373.
[17] R. d'Agostino, P. Favia, C. Oehr, M. R. Wertheimer, *Plasma Process. Polym.* **2005**, *2*, 7.
[18] K. Ostrikov, H.-J. Yoon, A. E. Rider, S. V. Vladimirov, *Plasma Process. Polym.* **2007**, *4*, 27.
[19] A. E. Rider, I. Levchenko, K. Ostrikov, *J. Appl. Phys.* **2007**, *101*, 044306.
[20] L. A. MacQueen, J. Zikovsky, G. Dennler, M. Latreche, G. Czeremuszkin, M. R. Wertheimer, *Plasma Process. Polym.* **2006**, *3*, 58.
[21] V. Ligatchev, Rusli, Z. Pan, *Appl. Phys. Lett.* **2005**, *87*, 242903.
[22] V. Ligatchev, *Physica B* **2003**, *337*, 333.
[23] S. Kicin, A. Pioda, T. Ihn, M. Sigrist, A. Fuhrer, K. Ensslin, M. Reinwald, W. Wegscheider, *New J. Phys.* **2005**, *7*, 185.
[24] S. J. Choi, M. J. Kushner, *J. Appl. Phys.* **1993**, *74*, 853.
[25] Y. Watanabe, M. Shiratani, K. Koga, *Plasma Sources Sci. Technol.* **2002**, *11*, A229.
[26] F. Rosei, R. Rosei, *Surf. Sci.* **2002**, *500*, 395.
[27] F. M. Ross, J. Tersoff, R. M. Tromp, *Phys. Rev. Lett.* **1998**, *80*, 984.
[28] T. L. Cottrell, "*The strength of chemical bonds*", Butterworths Publications Ltd, London 1958, p. 246.
[29] M. S. Silverberg, "*Chemistry: The molecular nature of matter and change*", McGraw-Hill, New York 2003, p. 339.
[30] "Properties of Solids", in *CRC Handbook of Chemistry and Physics*, Internet Version, D. R. Lide, Ed., Taylor and Francis, Boca Raton 2007, p. 12.
[31] J. D. Gale, J. M. Seddon, "*Thermodynamics and Statistical Mechanics*", Wiley-Interscience, New York 2002.
[32] H. J. Kim, Z. M. Zhao, J. Liu, V. Ozolins, J. Y. Chang, Y. H. Xie, *J. Appl. Phys.* **2004**, *95*, 6065.
[33] I. Levchenko, O. Baranov, *Vacuum* **2003**, *72*, 205.
[34] M. S. Valipa, T. Bakos, D. Maroudas, *Phys. Rev. B* **2006**, *74*, 205324.
[35] S. Gemmert, G. T. Barkema, S. Puri, *Phys. Rev. E* **2005**, *72*, 046131.
[36] R. Wetzler, R. Kunert, A. Wacker, E. Schöll, *New. J. Phys.* **2004**, *6*, 81.
[37] G. Fuchs, P. Melinon, F. Santos Aires, M. Treilleux, B. Cabaud, A. Hoareau, *Phys. Rev. B* **1991**, *44*, 3926.
[38] G. Fuchs, M. Treilleux, F. Santos Aires, B. Cabaud, P. Melinon, A. Hoareau, *Phys. Rev. A* **1989**, *40*, 6128.
[39] P. Roca i Cabarrocas, T. Nguyen-Tran, Y. Djeridane, A. Abramov, E. Johnson, G. Patriarche, *J. Phys. D: Appl. Phys.* **2007**, *40*, 2258.
[40] A. V. Dvurechenski, J. V. Smagina, R. Groetzschel, V. A. Zinovyev, V. A. Armbrister, P. L. Novikov, S. A. Teys, A. K. Gutakovskii, *Surf. Coat. Technol.* **2005**, *196*, 25.
[41] T. J. Krinke, K. Deppert, M. H. Magnusson, F. Schmidt, H. Fissan, *J. Aerosol Sci.* **2002**, *33*, 1341.
[42] I. Levchenko, K. Ostrikov, M. Keidar, S. Xu, *Appl.Phys.Lett.* **2006**, *89*, 033109.
[43] I. Levchenko, K. Ostrikov, E. Tam, *Appl. Phys. Lett.* **2006**, *89*, 223108.
[44] E. Tam, I. Levchenko, K. Ostrikov, *J. Appl. Phys.* **2006**, *100*, 036104.
[45] M. Keidar, A. M. Waas, *Nanotechnology* **2004**, *15*, 1571.
[46] M. Keidar, *J. Phys. D.: Appl. Phys.* **2007**, *40*, 2388.
[47] K. B. K. Teo, D. B. Hash, R. G. Lacerda, *Nano Lett.* **2004**, *4*, 921.
[48] Z. L. Tsakadze, K. Ostrikov, S. Xu, *Surf. Coat. Technol.* **2005**, *191*, 49.
[49] Z. L. Tsakadze, K. Ostrikov, J. D. Long, S. Xu, *Diamond Relat. Mat.* **2004**, *13*, 1923.
[50] I. B. Denysenko, S. Xu, P. P. Rutkevych, J. D. Long, N. A. Azarenkov, K. Ostrikov, *J. Appl. Phys.* **2004**, *95*, 2713.
[51] K. Ostrikov, A. B. Murphy, *J. Phys. D: Appl. Phys.* **2007**, *40*, 2223.
[52] T. Fukuzawa, S. Kushima, Y. Matsuoka, M. Shiratani, Y. Watanabe, *J. Appl. Phys.* **1999**, *86*, 3543.
[53] K. Ostrikov, J. D. Long, P. P. Rutkevych, S. Xu, *Vacuum* **2006**, *80*, 1126.
[54] K. Ostrikov, *IEEE Trans. Plasma. Sci.* **2007**, *35*, 127.
[55] I. Levchenko, A. E. Rider, K. Ostrikov, *Appl. Phys. Lett.* **2007**, *90*, 193110.
[56] S. Xu, K. Ostrikov, J. D. Long, S. Y. Huang, *Vacuum* **2006**, *80*, 621.
[57] I. Levchenko, K. Ostrikov, A. E. Rider, E. Tam, S. V. Vladimirov, S. Xu, *Phys. Plasmas* **2007**, *14*, 063502.
[58] K. N. Ostrikov, M. Y. Yu, H. Sugai, *J. Appl. Phys.* **1999**, *86*, 2425.
[59] K. N. Ostrikov, M. V. Yu, L. Stenflo, *Phys. Rev. E* **2000**, *61*, 782.